Electronic Supporting Information (ESI)

for

Interpenetrated N-rich MOF derived vesicular N-doped carbon for high performance lithium ion battery

Yun-Xiu Zhao,[a] Yuan-Wei Sun,[a] Jun Li,[a] Su-Na Wang,[a] Da-Cheng Li,[a] Jian-Min Dou,[a] Ming Zhong,[c] Hui-Yan Ma,*[,a] Yun-Wu Li*[,a] and Li-Qiang Xu*[,a,b]

[a] Shandong Provincial Key Laboratory of Chemical Energy Storage and Novel Cell Technology, and School of Chemistry and Chemical Engineering, Liaocheng University, Liaocheng 252000, P. R. China.

[b] Key Laboratory of Colloid and Interface Chemistry, Ministry of Education, and School of Chemistry and Chemical Engineering, Shandong University, Jinan 250100, P. R. China.

[c] State Key Laboratory of Advanced Processing and Recycling of Nonferrous Metals, Lanzhou University of Technology, Lanzhou 730050, P. R. China.

*To whom correspondence should be addressed.

E-mail: mahuiyanyan@163.com (H. Y. Ma); liyunwu@lcu.edu.cn (Y. W. Li); xulq@sdu.edu.cn (L. Q. Xu).

S1. Experimental Section

S1.1 Chemicals

The ligand (Hdctz) was synthesized according to the literature.[S1] All other chemicals were commercially purchased and used as received.

S1.2 Syntheses of $\{[Zn_{1.5}(dttz)(bpp)]\cdot H_2O\}_n$ (LCU-104)

A mixture of $ZnCl_2$ (68.15 mg, 0.5 mmol), NaN_3 (65 mg, 1 mmol), Hdcta (59.7 mg, 0.5 mmol) and bpp (59.4 mg, 0.3 mmol) in H_2O (8 mL) were sealed in a 23 mL Teflonlined stainless steel container, which was heated at 120 °C for 4 days and then cooled to room temperature at a rate of 10 °C·h^{-1}. Colourless block shaped crystals of **LCU-104** were collected. Yield: 52 % for **LCU-104** based on Zn, respectively. Elemental analysis (%) for **LCU-104**, $C_{17}H_{16}N_{13}OZn_{1.5}$ (M = 516.51): Calcd.: C, 39.53; H, 3.12; N, 35.25; Found: C, 39.42; H, 3.06; N, 35.33.

Caution. *Treated NaN_3 and Zn-tetrazolates compounds with great caution owing to their potentially explosive nature.*

S1.3 Preparation of vesicle-like N-doped porous carbon

The N/C was synthesized by direct carbonization of the as-prepared **LCU-104** under a flow of argon gas at a temperature of 800, 900 and 1000 °C (*abbr.* N/C-800, N/C-900, N/C-1000), respectively. Typically, the ground **LCU-104** was homogeneously dispersed in a ceramic boat and then placed into a tube furnace. After the sample was exposed to a flow of argon (400 mL·min^{-1}) at room temperature for 5 h, the furnace was heated to carbonization temperature 900 °C using a heating rate of 5 °C·min^{-1}. Then, the cooled resulting sample was extensively washed 3 times using a 3 M HCl to remove the residual Zn component. Next, the sample was washed several times with deionized water and absolute ethanol. After vacuum drying in an oven at 60 °C for 10 h, black powder of vesicle-like N/C material was obtained.

S1.4 Material Characterization

Elemental analyses (C, H and N) were performed on a Perkin-Elmer 2400 II analyzer (Perkin-Elmer, USA). The powder X-ray diffractions (PXRD) were obtained on a D/MAX-rA (Rigaku) diffractometer with Cu K_α radiation (λ = 1.542 Å) with a scan rate of 4° min^{-1}. The tube voltage and current are 36 kV and 20 mA, respectively. IR spectra were recorded on a FT6700 spectrometer (USA) using KBr disc method in the range of 400–4000 cm^{-1}. Simulation of the PXRD spectrum was carried out by the single-crystal data and diffraction-crystal module of the Mercury (Hg) program available free of charge *via* the Internet at http://www.iucr.org. Electron microscopy characterization of the samples was conducted using FESEM (field-emission scanning electron microscopy, Hitachi S-4800), TEM (transmission electron microscope, Hitachi H7700), and HRTEM (high-resolution transmission electron Microscopy, JEOL-2100F). Raman spectrum was measured using an Invia Raman Microscope (Invia Microscope, Renishaw, U.K.). XPS (X-ray photoelectron spectrum) of the sample was conducted using ESCALAB 250 instrument. The surface area and pore size distributions of the samples were acquired by the nitrogen adsorption/desorption apparatus (Quantachrome autosorb IQ-C).

S1.5 Electrochemical Measurements

The battery performance of the product was investigated using CR2032 coin cells using $LiPF_6$ in ethylene carbonate (EC), ethyl methyl carbonate (EMC), and diethyl carbonate (DEC) as the electrolyte (1 mol·L^{-1}, EC/EMC/DEC = 4:2:4, v/v/v). The working electrode was composed of 70 wt % active materials, 20 wt % carbon black (Super-P), and 10 wt % polyvinylidene fluoride (PVDF). The as-prepared slurry was then pasted onto the copper foil current collector, followed by vacuum drying (100 °C, 12 h). The tested cells were assembled in a glovebox filled with argon and then aged for 24 h before electrochemical test. The galvanostatic charge/discharge tests for the as-formed coin cells were carried out *via* LAND-CT2001A battery testers (voltage range: 0.01 to 3.00 V). Cyclic Voltammetry (CV) curves and electrochemical impedance spectroscopy (EIS) were measured using an electrochemical workstation (CHI660E, scan rate of 0.1 mV s^{-1}, potential window: 0.01−3.00 V).

S1.6 Computational Methods

The calculations were done within density functional theory (DFT) and plane wave pseudopotential technique, as implemented in the Vienna Ab-initio Simulation Package (VASP).[S2,S3] The generalized gradient approximation of Perdew-Burke-Ernzerhof (PBE)[S2,S3] for the exchange-correlation potential and the projector augmented wave (PAW) method[S2,S3] are employed in this code. As a simplified model of graphene sheet composed of 134 atoms ($C_{106}H_{28}$) was examined. The pristine graphene sheet is approximately 15 × 20 Å in size with all of the carbon atoms on the edges terminated with hydrogen atoms. The optimal defect model ($C_{99}H_{28}N_7$) was built by using seven N atoms to replace seven C atoms in the defects in the structure, which accords to the N content and the proportion of graphitic N and pyridinic N similar as N/C-900. In this model, the seven N atoms contain four graphitic N atoms and three pyridinic N atoms. The vacuum region between two graphene sheets was kept at 15 Å, which is thick enough for the system to converge to a correct total energy. A Γ-centered 1×1×2 Monkhorst-Pack grid for the Brillouin zone sampling and a cutoff energy of 400 eV for the plane wave expansion were found to get convergent lattice parameters.

S1.7 X-ray Crystallography

The crystallographic data of **LCU-104** were collected on a Rigaku SCX-mini diffractometer at 293(2) K with Mo-*K*α radiation (λ = 0.71073 Å). The crystal data were solved by direct methods and refined by a full-matrix least-square method on F^2 using the *SHELXL-97* crystallographic software package.[S4] Zn atoms in **LCU-104** were found from *E*-maps and other non-hydrogen atoms were located in successive difference Fourier syntheses. The final refinement was performed by full matrix least-squares methods with anisotropic thermal parameters for non-hydrogen atoms on F^2. The hydrogen atoms of organic ligands were added theoretically, riding on the concerned atoms and refined with fixed thermal factors. The H atoms of the lattice water molecule in **LCU-104** cannot be added in the calculated positions, and they were directly included in the final molecular formula. During the refinement of **LCU-104**, the command "omit -3 50" was used to omit some disagreeable reflections. Some commands

"DFIX" and "SIMU" were restrained to solve ADPs problems. The thermal ellipsoid diagram of **LCU-104** is shown in **Fig. S4**. Further details of crystal data and structure refinement for **LCU-104** were summarized as follow in **Table S1**. Full crystallographic data for **LCU-104** have been deposited with the CCDC (1471147). These data can be obtained free of charge from The Cambridge Crystallographic Data Centre *via* www.ccdc.cam.ac.uk/data_request/cif.[S5]

Crystal data for LCU-104.

Table S1. Crystal Data and Structure Refinement Parameters for LCU-104.

Compound	**LCU-104**
Formula	$C_{34}H_{30}N_{26}OZn_3$
F_w	1014.95
λ/Å	0.71073
T/K	293(2)
Crystal system	Tetragonal
Space group	$I4_1/a$
a [Å]	22.534(3)
b [Å]	22.534(3)
c [Å]	16.629(3)
α[°]	90
β [°]	90
γ[°]	90
V (Å^3)	8444(3)
Z	8
D_c/Mg·m^{-3}	1.597
F(000)	4112
Reflections collected/unique	35685/3720
R_{int}	0.0979
Data/Restraints/Parameters	3720/620/421
R_1/wR_2 [$I>2\sigma(I)$] [a]	0.0702/0.1545
R_1/wR_2 [(all data)] [a]	0.1144/0.1770
GOF on F^2	1.090
CCDC	1471147

S2. Figures in Supporting Information

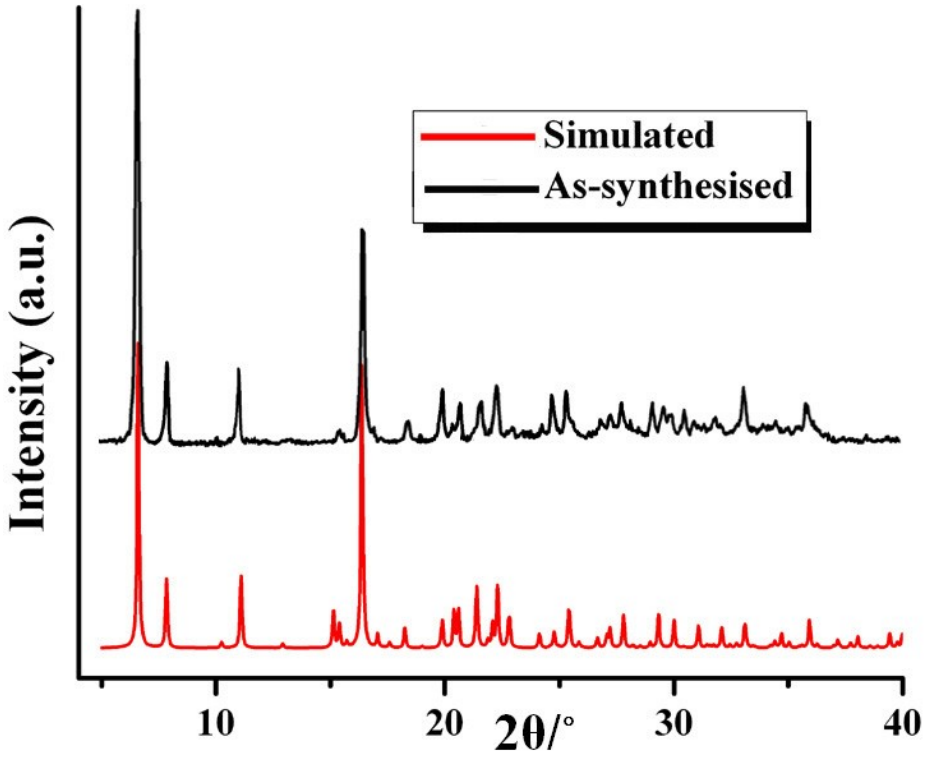

Fig. S1 PXRD patterns for **LCU-104**: (a) Simulated (red line). (b) As-synthesised (black line).

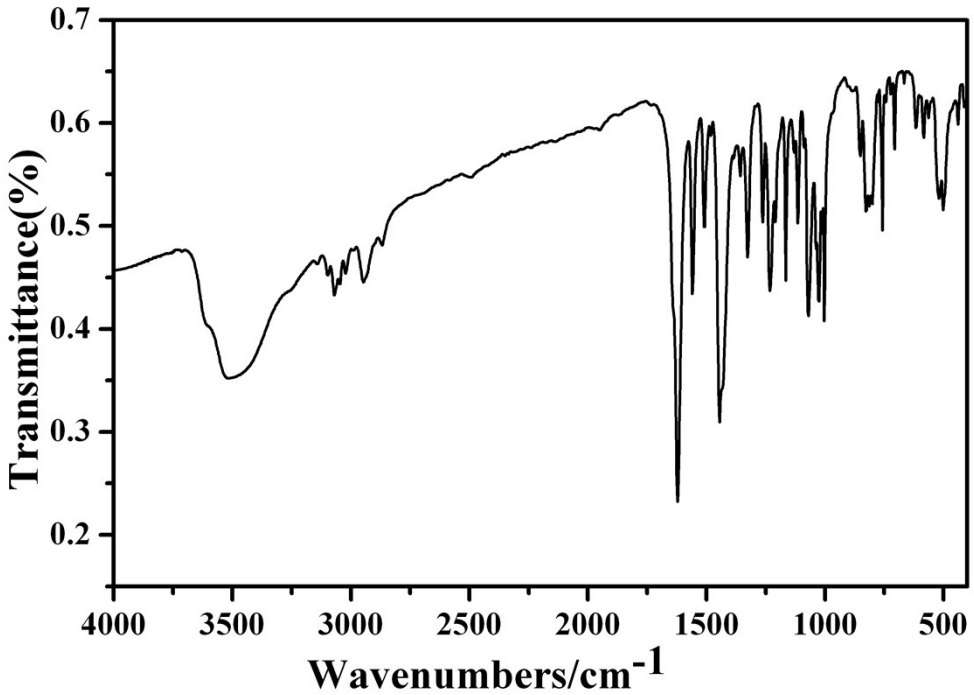

Fig. S2 IR spectrum of compound **LCU-104**.

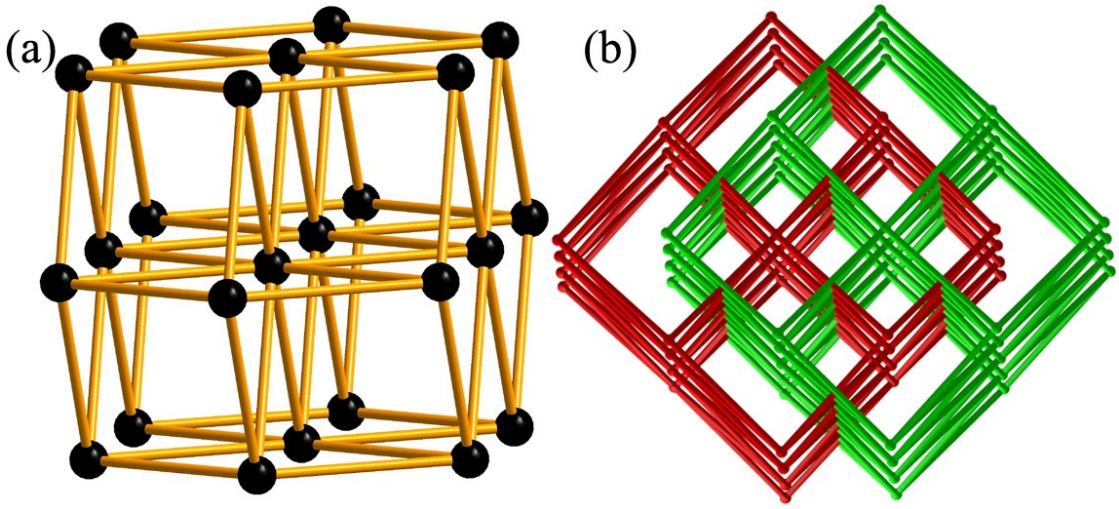

Fig. S3 (a) The individual **bcu** topology in **LCU-104**. (b) The two-fold interpenetrating **bcu** topology of **LCU-104**.

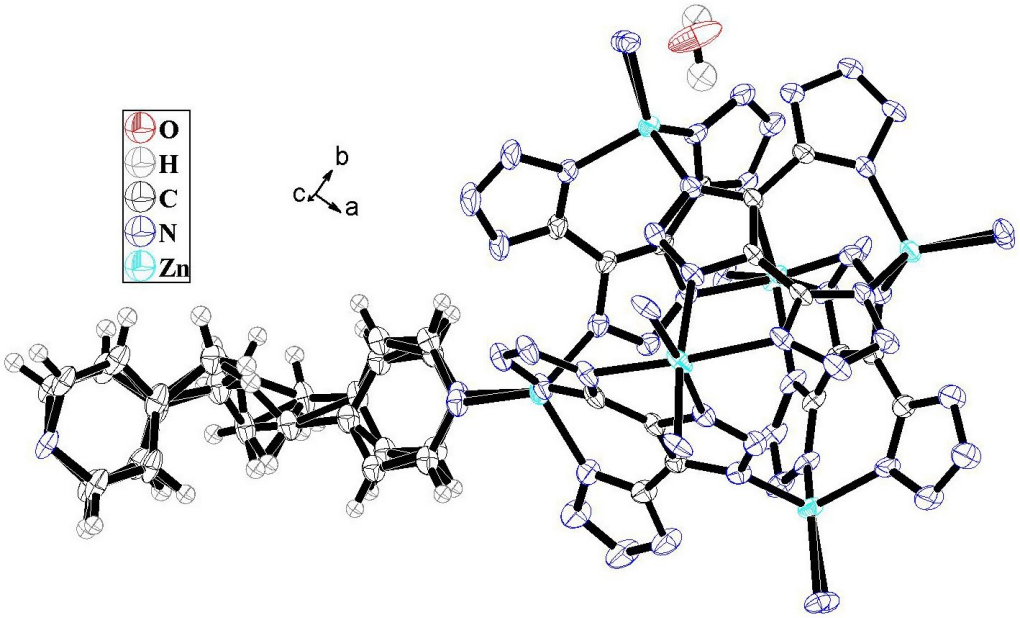

Fig. S4 The thermal ellipsoid diagram of **LCU-104**.

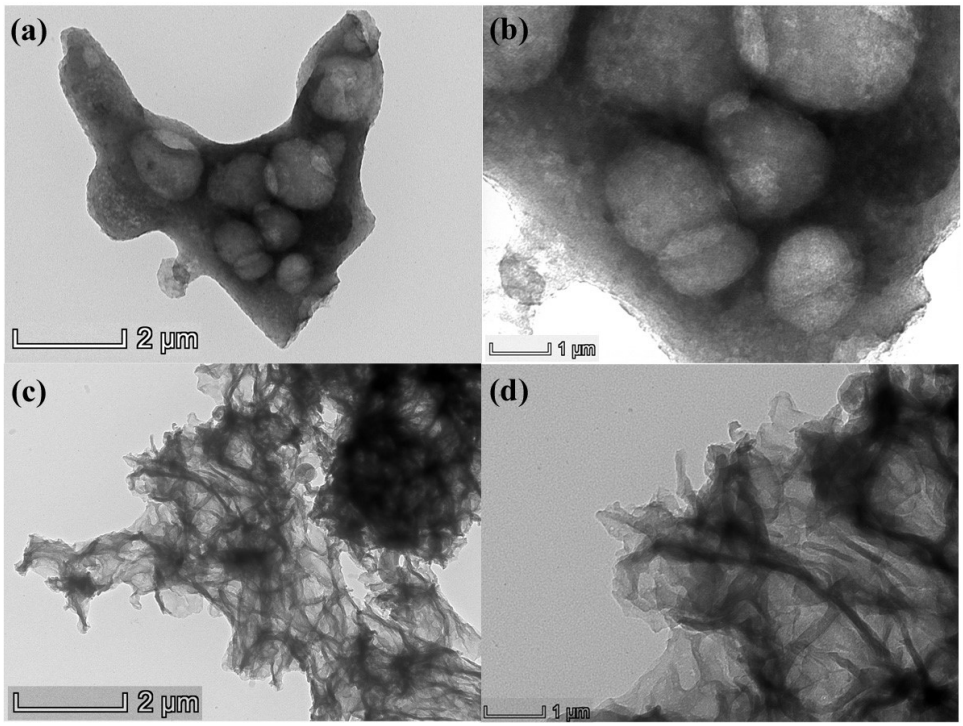

Fig. S5 (a) Low magnification TEM image of N/C-800. (b) Partially enlarged TEM image of N/C-800. (c) Low magnification TEM image of N/C-1000. (d) Partially enlarged TEM image of N/C-1000.

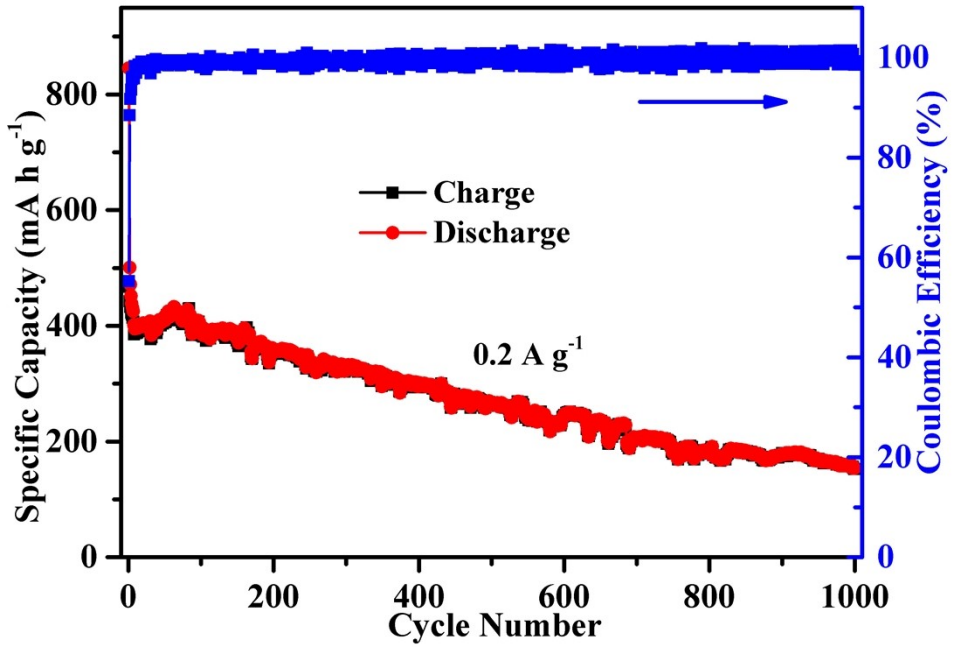

Fig. S6 Galvanostatic charge–discharge of cycling performance of N/C-800 at a current density of 0.2 A·g^{-1} until 1000th cycles.

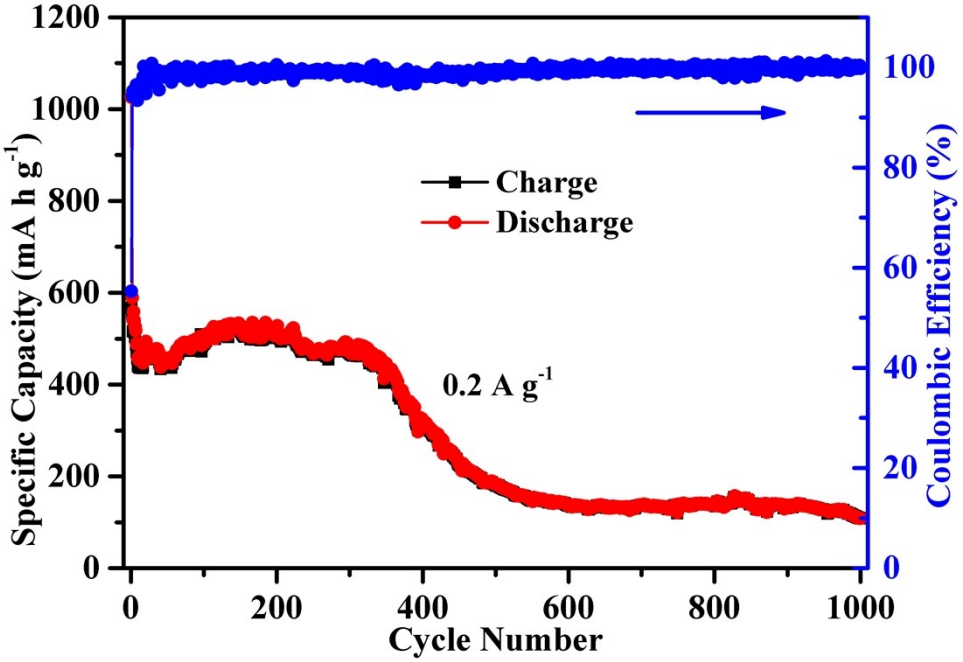

Fig. S7 Galvanostatic charge–discharge of cycling performance of N/C-1000 at a current density of 0.2 A·g^{-1} until 1000th cycles.

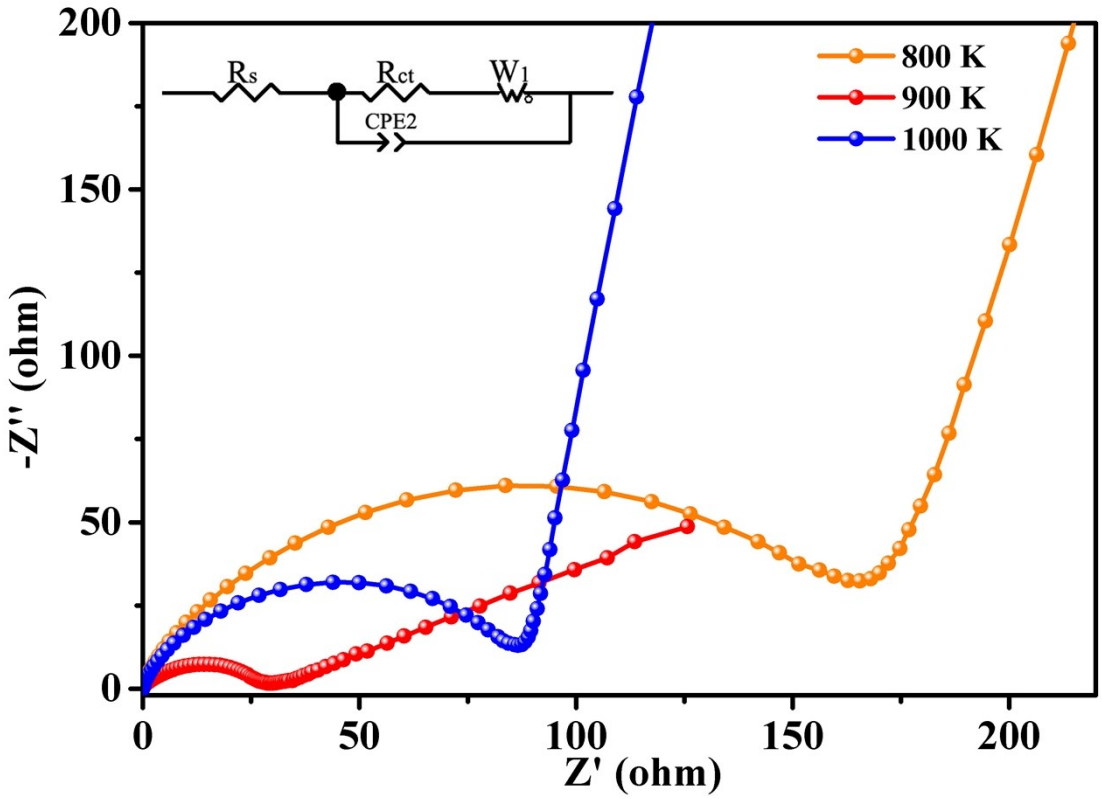

Fig. S8 EIS plots of three MOF derived catalysts (Inset: simulated equivalent circuit).

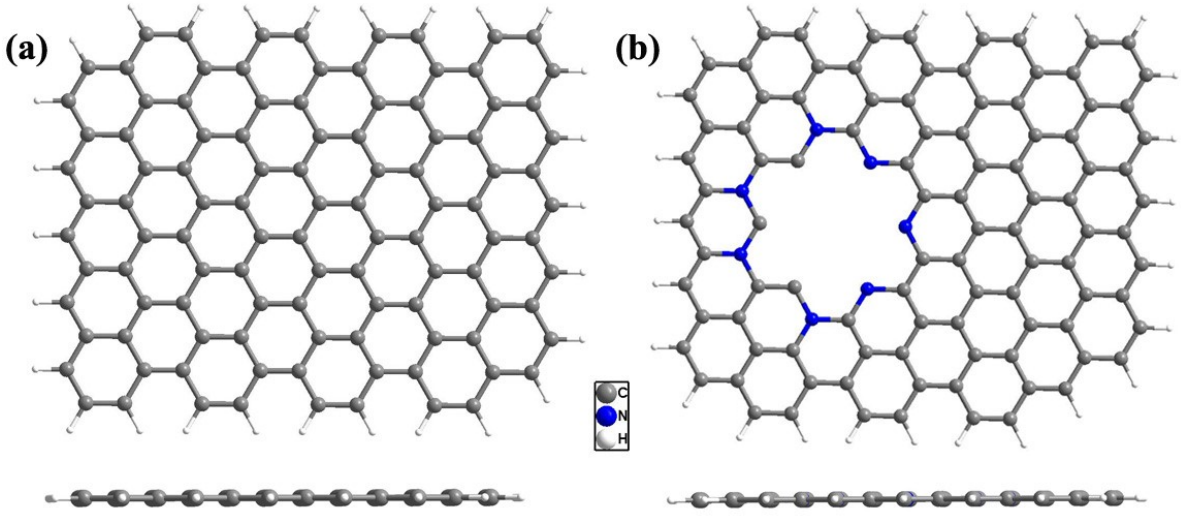

Fig. S9 (a) The pristine graphene model $C_{106}H_{28}$ both from top view and side view. (b) The optimal defect model ($C_{99}H_{28}N_7$) both from top view and side view. The gray, blue and white balls refer to carbon, nitrogen and hydrogen atoms, respectively.

S3. Table S2 A comparison of the capacity of this work with reported N-doped carbon materials for LIBs.

Samples	N-content	Current density (mA g^{-1})	Cycle number	Capacity (mA h g^{-1})	Refs.
LCU-104 derived N-doped carbon	6.58 wt%	1000	2000	734	This Work
NCH	19 wt%	1000	500	609	S6
PMC-850	6.04 wt%	500	100	460	S7
CNFWs	10.25 wt%	2000	600	943	S8
ZIF-8 Derived N-C-800	17.72 wt%	5000	1000	785	S9
CNT-CNF	1.4 wt%	100	70	1150	S10
HPCNT	8.2 wt%	1000	700	630	S11
CNTs	11.5 at.%	1000	400	850.1	S12
CNFs/CNTs	3.51 wt%	200	400	545	S13
N-ACAs	--	372	300	550	S14
NPCs	9.75 at.%	100	100	488	S15
N-carbon/rGO	15.4 wt%	500	1200	535	S16
N-doped graphene	7.04 at.%	50	50	1136	S17
HN-CNT	16.4 at.%	100	100	397	S18
GN	3.9 at.%	C/5	50	600	S19
NGr	2.8 at.%	2000	550	453	S20
GNS	2 at.%	42	10	900	S21
SnO_x/NC/C	6.20 wt%	1000	500	435	S22
Co_3O_4/N-C	2.27 at.%	1000	500	612	S23
N-d-SPC	4.7 at.%	50	100	673	S24
Zn_2SiO_4@NC	--	1000	400	540	S25
NCNS	10.6 wt%	1000	600	477	S26
N-OMC2	5.82 at.%	100	100	645.7	S27
NCS	--	20	500	580	S28

References

S1 M. J. Crawford, K. Karaghiosoff, T. M. Klapötke and F. A. Martin, Synthesis and characterization of 4,5-dicyano-2H-1,2,3-triazole and its sodium, ammonium, and guanidinium salts, *Inorg. Chem.*, 2009, **48**, 1731−1743.

S2 I. A. Courtney, J. S. Tse, O. Mao, J. Hafner and J. R. Dahn, *Ab initio* calculation of the lithium-tin voltage profile, *Phys. Rev. B*, 1998, **58**, 15583.

S3 K. Persson, Y. Hinuma, Y. S. Meng, A. Van der Ven and G. Ceder, Thermodynamic and kinetic properties of the Li-graphite system from first-principles calculations, *Phys. Rev. B*, 2010, **82**, 125416.

S4 (a) G. M.Sheldrick, *SHELXL97, Program for Crystal Structure Refinement*; University of Göttingen: Göttingen, Germany, 1997; (b) G. M. Sheldrick, *SHELXS97, Program for Crystal Structure Solution*; University of Göttingen: Göttingen, Germany, 1997.

S5 The checkcif program available at: http://journals.iucr.org/services/cif/checkcif.html.

S6 X. G. Han, L. M. Sun, F. Wang and D. Sun, MOF-derived honeycomb-like N-doped carbon structures assembled from mesoporous nanosheets with superior performance in lithium-ion batteries, *J. Mater. Chem. A*, 2018, **6**, 18891−18897.

S7 Z. Li, Z. W. Xu, X. H. Tan, H. L. Wang, C. M. B. Holt, T. Stephenson, B. C. Olsen and D. Mitlin, Mesoporous nitrogen-rich carbons derived from protein for ultra-high capacity battery anodes and supercapacitors, *Energy Environ Sci.*, 2013, **6**, 871−878.

S8 L. Qie, W. M. Chen, Z. H. Wang, Q. G. Shao, X. Li, L. X. Yuan, X. L. Hu, W. X. Zhang and Y. H. Huang, Nitrogen-doped porous carbon nanofiber webs as anodes for lithium ion batteries with a superhigh capacity and rate capability, *Adv. Mater.*, 2012, **24**, 2047−2050.

S9 F. C. Zheng, Y. Yang and Q. W. Chen High lithium anodic performance of highly nitrogen-doped porous carbon prepared from a metal-organic framework, *Nat. Commun.*, 2014, **5**, 5261.

S10 Y. M. Chen, X. Y. Li, K. Park, J. Song, J. H. Hong, L. M. Zhou, Y. W. Mai, H. T. Huang and J. B. Goodenough, Hollow carbon-nanotube/carbon-nano fiber hybrid anodes for Li-ion batteries, *J. Am. Chem. Soc.*, 2013, **135**, 16280−16283.

S11 J. Lin, Y. L. Xu, J. Wang, B. F. Zhang, D. Li, C. Wang, Y. L. Jin and J. B. Zhu, Nitrogen-doped hierarchically porous carbonaceous nanotubes for lithium ion batteries, *Chem. Eng. J.*, 2018, **352**, 964−971.

S12 H. I. Cho, Y. C. Jeong, J. H. Kim, Y. S. Cho, T. Kim, S. J. Yang and C. R. Park, Rational design of 1D partially graphitized N-doped hierarchical porous carbon with uniaxially packed carbon nanotubes for high-performance lithium-ion batteries, *ACS Nano*, 2018, **12**, 11106−11119.

S13 L. Huang, Q. Guan, J. L. Cheng, C. Li, W. Ni, Z. P. Wang, Y. Zhang and B. Wang, Free-standing N-doped carbon nanofibers/carbon nanotubes hybrid film for flexible, robust half and full lithium-ion batteries, *Chem. Eng. J.*, 2018, **334**, 682−690.

S14 J. L. Zhang, L. J. Zhang, S. L. Yang, D. H. Li, Z. X. Xie, B. B. Wang, Y. Z. Xia and F. Y. Quan, Facile strategy to produce N-doped carbon aerogels derived from seaweed for lithium-ion battery anode, *J. Alloy. Compd.*, 2017, **701**, 256−261.

S15 X. J. Zhang, G. Zhu, M. Wang, J. B. Li, T. Lu and L. K. Pan, Covalent-organic-frameworks derived N-doped porous carbon materials as anode for superior long-life cycling lithium and sodium ion batteries, *Carbon*, 2017, **116**, 686−694.

S16 X. H. Liu, J. Zhang, S. J. Guo and N. Pinna, Graphene/N-doped carbon sandwiched nanosheets with ultrahigh nitrogen doping for boosting lithium-ion batteries, *J. Mater. Chem. A*, 2016, **4**, 1423−1431.

S17 D. D. Cai, S. Q. Wang, P. C. Lian, X. F. Zhu, D. D. Li, W. S. Yang and H. H. Wang, Superhigh capacity and rate capability of high-level nitrogen-doped graphene sheets as anode materials for lithium-ion batteries, *Electrochim. Acta*, 2013, **90**, 492−497.

S18 X. F. Li, J. Liu, Y. Zhang, Y. L. Li, H. Liu, X. B. Meng, J. L. Yang, D. S. Geng, D. N. Wang, R. Y. Li and X. L. Sun, High concentration nitrogen doped carbon nanotube anodes with superior Li^+ storage performance for lithium rechargeable battery application, *J. Power Sources*, 2012, **197**, 238−245.

S19 X. Wang, Q. H. Weng, X. Z. Liu, X. B. Wang, D. M. Tang, W. Tian, C. Zhang, W. Yi, D. Q. Liu, Y. Bando and D. Golberg, Atomistic origins of high rate capability and capacity of N-doped graphene for lithium storage, *Nano Lett.*, 2014, **14**, 1164−1171.

S20 T. Hu, X. Sun, H. T. Sun, G. Q. Xin, D. L. Shao, C. S. Liu and J. Lian, Rapid synthesis of nitrogen-doped graphene for a lithium ion battery anode with excellent rate performance and super-long cyclic stability, *Phys. Chem. Chem. Phys.*, 2014, **16**, 1060−1066.

S21 H. B. Wang, C. J. Zhang, Z. H. Liu, L. Wang. P. X. Han, H. X. Xu, K. J. Zhang, S. M. Dong, J. H. Yao and G. L. Cui, Nitrogen-doped graphene nanosheets with excellent lithium storage properties, *J. Mater. Chem.*, 2011, **21**, 5430−5434.

S22 C. Zhu, D. H. Wei, Y. L. Wu, Z. Zhang, G. H. Zhang, J. F. Duan, L. J. Li, H. L. Zhu, Z. Y. Zhu and Z. Y. Chen, Controllable construction of interconnected SnOx/N-doped carbon/carbon composite for enhanced-performance lithium-ion batteries Anodes, *J. Alloy. Compd.*, 2019, **778**, 731−740.

S23 X. Han, W. M. Chen, X. G. Han, Y. Z. Tan and D. Sun, Nitrogen-rich MOF derived porous Co_3O_4/N–C composites with superior performance in lithium-ion batteries, *J. Mater. Chem. A*, 2016, **4**, 13040−13045.

S24 R. Z. Li, J. F. Huang, J. Y. Li, L. Y. Cao, X. Z. Zhong, A. M. Yu and G. X. Lu, Nitrogen-doped porous hard carbons derived from shaddock peel for high capacity lithium-ion battery anodes, *J. Electroanal. Chem.*, 2020, **862**, 114044.

S25 F. Liu, S. Y. Liu, J. S. Meng, F. J. Xia, Z. T. Xiao, Z. A. Liu, Q. Li, J. S. Wu and L. Q. Mai, Stabilizing conversion reaction electrodes by MOF derived N-doped carbon shell for highly reversible lithium storage, *Nano Energy*, 2020, **73**, 104758.

S26 T. Kesavan and M. Sasidharan, Palm spathe derived N-doped carbon nanosheets as a high performance electrode for Li-ion batteries and supercapacitors, *ACS Sustain. Chem. Eng.*, 2019, **7**, 12160−12169.

S27 H. T. T. Le, T. D. Dang, N. T. H. Chu and C. J. Park, Synthesis of nitrogen-doped ordered mesoporous carbon with enhanced lithium storage performance from natural kaolin clay, *Electrochim, Acta*, 2020, **332**, 135399.

S28 H. W. Zhang, M. X. Hu, Q. Lv, L. Yang and R. T. Lv, Monodisperse nitrogen-doped carbon spheres with superior rate capacities for lithium/sodium ion storage, *Electrochim. Acta*, 2019, **297**, 365−371.